Molecular Vision 2018; 24:853-866 <http://www.molvis.org/molvis/v24/853>
Received 9 August 2018 | Accepted 29 December 2018 | Published 29 December 2018

Immunophenotypic characterization of telocyte-like cells in pterygium

Cristina Maxia,[1] Daniela Murtas,[1] Michela Isola,[1] Roberto Tamma,[2] Ignazio Zucca,[3] Franca Piras,[1] Domenico Ribatti,[2] Andrea Diana,[1] Maria Teresa Perra[1]

(The first two authors contributed equally to this work)

(The last two authors are co-senior authors for this study.)

[1]Department of Biomedical Sciences, University of Cagliari, Italy; [2]Department of Basic Medical Sciences, Neurosciences and Sensory Organs, University of Bari, Italy; [3]Department of Surgical Science, Eye Clinic, University of Cagliari, Italy

Purpose: Telocytes (TCs) are peculiar interstitial cells, characterized by their typical elongated and interconnected processes called telopodes. TCs are supposed to contribute to maintain tissue homeostasis but also to be involved in the pathophysiology of many disorders. The aim of the study was to identify TCs in pterygium, a chronic condition of bulbar conjunctiva, and to examine possible differences in TCs in terms of immunophenotype and/or localization between pterygium and normal conjunctiva, to evaluate the possible involvement of TCs in pathogenesis of pterygium.
Methods: The analysis of the immunophenotype of TCs was performed on a group of 40 formalin-fixed and paraffin-embedded primary pterygium and ten bulbar conjunctiva samples. We examined with immunohistochemistry the expression of 11 commercially available antibodies (PDGFRα, CD34, c-kit, nestin, vimentin, α-SMA, laminin, S100, VEGF, CD133, and CD31) and with double immunofluorescence the concomitant expression of PDGFRα and CD34, and PDGFRα and nestin. In addition, we performed an ultrastructural study with transmission electron microscopy (TEM) on a group of five pterygium and three conjunctiva biopsy specimens.
Results: TCs, ultrastructurally identified according to their "moniliform" prolongations, were localized underneath the epithelium along the basement membrane, around the vessels, and near the nerves and scattered in the stroma. In contrast, TCs, as fibroblasts, were almost absent in the fibrotic areas. In pterygium and normal conjunctiva, the TCs shared the same distribution pattern, except a marked TC hyperplasia detected in pterygium. Moreover, in pterygium, the immunohistochemical analysis of TCs showed a strong immunoreactivity to PDGFRα, CD34, and nestin. This result was confirmed with double immunofluorescence labeling, revealing that in pterygium stromal TCs always showed a PDGFRα+/nestin+ and PDGFRα+/CD34+ immunophenotype. Furthermore, moderate staining to vimentin and VEGF was detected, but only a small number of cells were weakly immunoreactive to laminin and S100. Only adventitial TCs of the perivascular sheaths exhibited strong immunoreactivity to α-SMA. Conversely, despite showing mild immunoreactivity to PDGFRα and CD34, the TCs in normal conjunctiva did not show any immunoreactivity to nestin and VEGF. Moreover, in pterygium and conjunctiva, the TCs were always negative for c-kit.
Conclusions: Because of the distribution and immunophenotype, TCs in pterygium may represent a subpopulation of relatively immature cells with regenerative potential. In addition, the expression of nestin may suggest possible involvement of TCs as active players in the regeneration of ultraviolet-damaged stroma and vascular remodeling. The fibrotic transformation in the cicatricial area may stand for a breakdown of the regenerative process.

First described as interstitial Cajal-like cells, telocytes (TCs) are a peculiar interstitial cell type, discovered by serendipity in 2010 [1] and then identified in many vertebrate tissues and organs [2]. The name derives from the cells' extremely elongated, thin, tortuous, overlapping, and interconnected processes called telopodes (Tps), which form a typical three-dimensional network within the stroma. TCs are optimal candidates for maintaining tissue homeostasis thanks to their strategic position in relation to stem cell niches, capillaries, and nerves. TCs are meant to be "connecting cells" [3], because of their driving function in intercellular signaling by "stromal synapses" [4] and therefore, have drawn the attention of the scientific community for possible involvement in the pathophysiology of several disorders.

In the last few years, numerous papers have been published about this topic (telocytes). Transmission electron microscopy (TEM) seems to be the elective method for identifying TCs, although it has been widely demonstrated that immunohistochemistry alone is not sufficient to characterize TCs. A unique marker that universally recognizes TCs has

Correspondence to: Cristina Maxia, Department of Biomedical Sciences, Section of Cytomorphology, University of Cagliari, Cittadella Universitaria, 09042 Monserrato (CA), Italy; Phone. +39 070 6754005; FAX: +39 070 6754003; email: cmaxia@unica.it

not been identified thus far, because the TC immunophenotype might be strictly dependent on the location and needs of the tissue.

In particular, only a few papers have focused on the presence of TCs in the eye [5,6]. Luesma and colleagues detected interstitial cells with typical features of TCs in the lamina propria of mouse conjunctiva, but at present, no detailed information about immunophenotype and localization is available, in either healthy or pathologic human conjunctiva. A common disorder of bulbar conjunctiva is the chronic, degenerative, and hyperplastic condition called pterygium, a wing-shaped or triangular overgrowth of conjunctival mucosa that extends centripetally on the cornea. Pterygium is characterized by inflammatory features, marked neoangiogenesis, epithelial cell proliferation, and elastoid and basophilic degeneration of the subepithelial connective tissue [7]. There is consensus among researchers that pterygium is a type of benign disease, which, however, exhibits the typical features of a tumoral process. Because of pterygium's aggressiveness in recurrence after removal and tendency to invade the cornea leading to visual loss and diplopia [8] and to show several degrees of histopathological changes (extending from mild dysplasia to carcinoma in situ), the disease is now mostly considered a neoplastic-like growth disorder [9,10]. Moreover, some studies demonstrated an association between pterygium and preneoplastic lesions, such as primary acquired melanosis with atypia (PAM) [11,12]. About pathogenesis of pterygium, ultraviolet radiation (UVR) seems to have a key role in the development of pterygium, although a plethora of risk factors, such as extracellular matrix remodeling [13], inflammatory process [14-16], antiapoptotic mechanisms [17], cytokines [18], growth and angiogenic factors [19,20], viral infections [21], oxidative stress [22], hypoxic ischemic injury [23], anomaly in epithelial differentiation [24], and defects in vitamin D and vitamin D receptor pathways [25], have been proposed as causative agents. Moreover, possible involvement of bone marrow–derived progenitor cells has been suggested [26-28].

Based on previous observations by several authors in identifying TCs in cavitary and parenchymatous organs, the purpose of the present study was to identify TCs in pterygium stroma and to investigate their immunophenotype and/or localization. Results highlighting possible differences between normal conjunctival mucosa and pterygium could be useful to better understand the pathogenesis of the lesion.

METHODS

Patients and study design: The study was performed on a group of 45 pterygium samples obtained from patients (32 men and 13 women, age ranging from 28 to 82 years) who underwent surgery for pterygium removal at the Department of Surgical Science, Eye Clinic of the University of Cagliari. Most pterygia were located on the nasal side (33.73%). The morphology was clinically graded as atrophic (12, 27%), intermediate (27, 60%), or fleshy (6, 13%) according to an assessment of pterygium translucency, and included 29 (64%) inflamed and 16 (36%) quiescent lesions. Moreover, 13 normal epibulbar conjunctiva samples, used as control tissues, were excised near the limbus from healthy donors (five men and eight women, age ranging from 13 to 77 years), with no signs or symptoms of pterygium or ocular surface disorder, during cataract surgery.

The study was conducted in adherence to the ARVO Statement on human subjects and was approved by the local Institutional Ethic Committee, and written consent was obtained from all patients before the beginning of the study, according to the Declaration of Helsinki. Patients did not receive any medication before surgery, except topical anesthetic; demographic and clinical information on patients, available in all cases, is reported in Table 1.

Immunohistochemistry: Among the group of 45 pterygium samples, 40 specimens were 10% formalin-fixed and processed for paraffin embedding; moreover, ten epibulbar conjunctiva biopsy, among the group of 13 samples from healthy donors, were fixed in formalin, embedded in paraffin, and used as normal controls. Three microtome histological sections (6–7 µm thick) per sample were treated for the immunohistochemical analysis of 11 antigens (Table 2) with the streptavidin-biotin alkaline phosphatase method, as previously described [25]. They were dewaxed, rehydrated, and rinsed in PBS (1X; 120 mM NaCl, 20 mM KCl, 10 mM $NaPO_4$, 5 mM KPO_4, pH 7.4). When needed, water bath heating-based antigen retrieval was performed by immersion in Tris 10 mM and EDTA 1 mM (pH 9.0) for 20 min, or in citrate buffer, 10 mM (pH 6.0) for 30 min, or Tris 0.5 M (pH 10.0) for 30 min at 95 °C, followed by cooling for 20 min at room temperature (RT). Proteolytic antigen retrieval was obtained with immersion in a solution containing 0.1% Trypsin (Difco, Becton, Dickinson and Company, Sparks, MD), at 37 °C for 5 or 10 min. Furthermore, sections were treated for 45 min at RT with 10% non-immune serum to block non-specific binding and then incubated with the primary antibodies for 1 h at RT or overnight at 4 °C. The sources, dilutions, time of incubation, and details of the primary antibodies used for the immunohistochemical

staining, according to the Resource Identification Initiative, are reported in Table 2 [29]. Biotinylated anti-mouse, anti-rabbit, or anti-goat was used as secondary antisera (1:200; Vector Laboratories, Burlingame, CA) and incubated for 30 min at RT. The sections were further incubated in alkaline phosphatase streptavidin (1:1,000, Vector Laboratories) for 30 min at RT and reacted with the SIGMAFAST™ Fast red substrate–chromogen system (Sigma, St. Louis, MO). All sections were thoroughly rinsed in PBS between each step and counterstained with Carazzi hematoxylin and mounted in glycerol gelatin (Sigma).

Sections of archival human biopsy specimens were used as positive controls: terminal ileum for PDGFRα; tonsil for CD34; skin for c-kit, vimentin, α-SMA, and laminin; and known-positive melanoma for nestin, S-100, VEGF, CD133, and CD31. Negative controls were obtained by omitting the primary antibody or by replacing the primary antibody with an isotype-matched antibody. Positive and negative controls were run simultaneously.

Immunolabeled slides were imaged using a Zeiss Axioplan2 microscope (Carl Zeiss Vision, Hallbergmoos, Germany) equipped with the following objectives: 4X/0.10, 10X/0.25, 20X/0.45 Zeiss Achroplan; 40X/0.75 Zeiss Plan-Neofluar; 63X/1.40 oil immersion Zeiss Plan-Apochromat, and 100X/1.25 oil immersion Zeiss Achroplan. The images were acquired with a Lumenera Infinity 3–1URC camera (1.4 megapixels; Lumenera Corporation, Ottawa, Canada) and Infinity Capture 6.3.0 software (Lumenera Corporation). Adobe Photoshop CS3 Extended (ver. 10.0; Adobe Systems Inc., San Jose, CA) was used to set up the figure panels and for slight adjustments of brightness and contrast.

Scoring: Immunoreactivity was independently assessed by two experienced observers (CM and DM) in a blinded fashion. In each of the three sections per sample, the immunoreactivity was scored semiquantitatively (+++, ++, +, and ±, for strong, moderate, mild, and weak, respectively; - stands for absence of staining) [30] in four to six randomly chosen microscopic fields (40X original magnification).

Double immunofluorescence: A simultaneous procedure, as previously described [31,32], was used for the double staining of PDGFRα and CD34, and PDGFRα and nestin. Following deparaffinization, rehydration, antigen retrieval, and blocking of nonspecific binding, sections of pterygium and conjunctiva were incubated overnight at 4 °C with a mixture of goat polyclonal anti-human PDGFRα (1:50, R&D Systems Inc., Minneapolis, MN) and mouse monoclonal anti-human CD34 (1:50; Santa Cruz Biotechnology Inc., Dallas, TX) or mouse monoclonal anti-human nestin (1:100; Novus Biologicals, Littleton, CO) primary antibodies. Donkey Alexa Fluor 488 anti-goat immunoglobulin G (H+L) and Alexa Fluor 594 anti-mouse IgG (H+L) (1:500 and 1:200, respectively; Invitrogen Life Technologies, Paisley, UK) secondary antibodies were used for immunofluorescence detection. The sections were mounted in Vectashield mounting medium with 4′,6-diamidino-2-phenylindole (DAPI) to visualize nuclear details (Vector Laboratories). Immunofluorescence-labeled

Table 1. Clinical features of the patients.

Clinical variables	Pterygium (n. 45)	Conjunctiva (n. 13)
Mean age (±SD)	58.27 (±14.06)	37.48 (±18.85)
Age range (yrs)	28-82	13-77
Sex (%)		
Male	32 (71)	5 (38)
Female	13 (29)	8 (62)
Location of the lesion (M/F)		
Nasal side	33 (22/11)	
Temporal side	12 (10/2)	
Grade (%)		
Atrophic	12 (27)	
Intermediate	27 (60)	
Fleshy	6 (13)	
Disease stage (%)		
Inflamed	29 (64)	
Quiescent	16 (36)	

sections were imaged using a Zeiss Axioplan2 microscope (HBO 100 illuminator; mercury vapor, short arc lamp) equipped with the appropriate filter sets to distinguish the chosen fluorochromes and the objectives and digital camera mentioned above. The displayed figure panel was set up with Adobe Photoshop; only slight adjustments of brightness and contrast were performed.

Transmission electron microscopy: Five pterygium samples (among the group of 45) and three bulbar conjunctiva biopsies (among the group of 13) were used for the ultrastructural analysis as previously described [33]. The specimens were cut into small pieces and fixed for 2 h at RT with a mixture of 1% paraformaldehyde and 1.25% glutaraldehyde in 0.1 M cacodylate buffer (pH 7.2). Then, they were rinsed in cacodylate buffer with 3.5% sucrose added, fixed with osmium tetroxide, dehydrated, and embedded in Epon Resin (Glycidyl Ether 100; Merck, Darmstadt, Germany). Randomly selected tissue blocks from each patient were used to prepare sections for light and electron microscopic studies. Semithin sections stained with toluidine blue were observed and captured with the microscope Zeiss Axioplan2 to check the histological appearance. Ultrathin sections (90–100 nm) were cut with a diamond knife, collected on grids, stained with uranyl acetate and bismuth subnitrate, and observed and randomly photographed under a JEOL 100S (Tokyo, Japan) transmission electron microscope.

RESULTS

TCs, morphologically identified by their elongated and moniliform prolongations, in pterygium were localized underneath the epithelium along the basement membrane and in the lamina propria (Figure 1A,B,E,F,I,K); in the stromal compartment, the TCs were widespread and arranged in perivascular sheaths around the newly formed vessels (Figure 1A,B,E–G,J), and near the nerves and scattered in the stroma, where they ran in bundles, parallel to the epithelium and resembling the elastic fiber orientation (Figure 1A,E,J). Pterygium and normal conjunctiva shared the same TC distribution pattern; however, in pterygium marked stromal TC hyperplasia was detected (Figure 1A,E,J). In addition, in certain areas, the arrangement in parallel bundles went missing and was replaced with a wide TC network (Figure 1E). In those areas of pterygium in which the degeneration of the elastic fibers reached the highest level, the stroma became fibrotic, and turned into cicatricial tissue, where TCs and fibroblasts were almost absent (Figure 1C). On the border of the cicatricial area, a group of stellate TCs, with at least five extremely long, branched, dendritic-like processes, was observed (Figure 1C).

Table 2. Primary antibodies used in the study.

Target	Primary antibody						Biotinylated secondary antibody
	vendor	origin	dilution	incubation	antigen retrieval	RRID*	
PDGFRa	R&D Systems	Goat (pc)	1:200	O.N.	Heat-induced[1]	AB_354459	Horse anti-goat IgG[6]
CD34	Santa Cruz Biotechnology	Mouse (QBEnd/10)	1:100	1 h. RT	n.r.	AB_629044	Horse anti-mouse IgG[6]
c-kit	DAKO	Rabbit (pc)	1:200	1 h. RT	Heat-induced[2]	AB_2335702	Goat anti-rabbit IgG[6]
Nestin	Novus Biologicals	Mouse (10C2)	1:1000	1 h. RT	n.r.	AB_10001441	Horse anti-mouse IgG[6]
Vimentin	Millipore	Goat (pc)	1:2500	1 h. RT	n.r.	AB_90774	Horse anti-goat IgG[6]
α-SMA	Abcam	Rabbit (pc)	1:500	1 h. RT	n.r.	AB_2223021	Goat anti-rabbit IgG[6]
Laminin	Novus Biologicals	Rabbit (pc)	1:500	O.N.	Proteolytic[3]	AB_10001146	Goat anti-rabbit IgG[6]
S-100	DAKO	Rabbit (pc)	1:1000	1 h. RT	Proteolytic[3]	AB_10013383	Goat anti-rabbit IgG[6]
VEGF	Santa Cruz Biotechnology	Rabbit (pc)	1:500	O.N.	Proteolytic[4]	AB_2212984	Goat anti-rabbit IgG[6]
CD133	Abcam	Rabbit (pc)	1:1000	1 h. RT	Proteolytic[4]	AB_470302	Goat anti-rabbit IgG[6]
CD31	DAKO	Mouse (JC70A)	1:50	1 h. RT	Heat-induced[5]	AB_2114471	Horse anti-mouse IgG[6]

Pc, polyclonal. mc, monoclonal. O.N., overnight. RT, room temperature. n.r., not required. Water bath heating-based antigen retrieval at 95 °C in [1]TRIS 10mM + EDTA 1mM (pH 9.0) for 20 min; [2]citrate buffer, 10mM (pH 6.0) for 30 min; [5]TRIS 0.5M (pH 10.0) for 30 min. Proteolytic pre-treatment with Trypsin (Difco, Becton, Dickson and Company, MD), 0.1% 37 °C for 5 min[3] or 10 min[4]. [6]Vector Laboratories, Burlingame, CA. *The Resource Identification Initiative (Bandrowski et al. 2015); Resource Identification Portal.

The analysis of the immunophenotype of the TCs (Table 3) in pterygium displayed strong immunostaining for PDGFRα (Figure 1A–C), CD34 (Figure 1E–G), and nestin (Figure 1I–K), sharing a similar distribution pattern. PDGFRα-, CD34-, and nestin-positive TCs were detected in the connective stroma, around the vessels, along the basement membrane, and scattered in the stroma with long interconnected Tps (Figure 1). The immunohistochemical results were confirmed with double immunofluorescence labeling, revealing that in pterygium stromal TCs always showed a PDGFRα+/nestin+ (Figure 2A–C) and PDGFRα+/CD34+ (Figure 2E–G) immunophenotype. Nestin was always expressed in a punctate/granular pattern (Figure 2B,C). The scattered conjunctival stromal TCs always showed a PDGFRα+/nestin- (Figure 2D) and PDGFRα+/CD34+ (Figure 2H) immunophenotype.

Telocytes also showed moderate immunoreactivity to vimentin (Figure 3C) and VEGF (Figure 3D), and weak staining to S100 (Figure 3E) and laminin (Figure 3F) in stromal telocyte-like cells was detected. S100-positive TCs were scattered in the lamina propria of pterygium, showing immunoreactivity less intense than that of the internal controls, represented by stromal nerves, epithelial melanocytes, and Langerhans' cells. CD133 immunoreactivity in TCs was totally absent and limited to endothelial cells of pterygium neoformed blood vessels (Figure 3I), which showed immunostaining also for CD31 (Figure 3K), PDGFRα (Figure 1B), CD34 (Figure 1E–G), nestin (Figure 1I,J), vimentin (Figure 3C), and VEGF (Figure 3D). TCs did not display any staining for CD31 (Figure 3K).

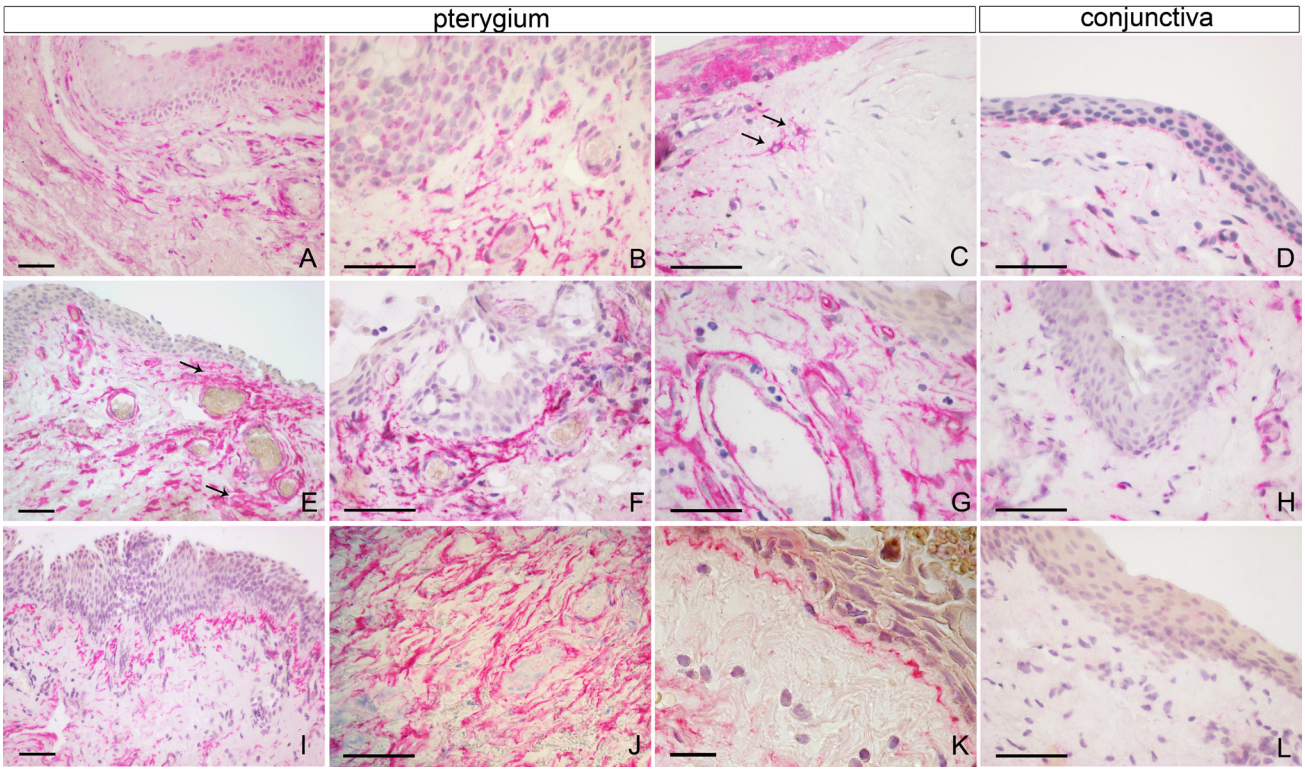

Figure 1. Distribution of PDGFRα-, CD34-, and nestin-immunoreactive TCs in pterygium and conjunctiva. **A**–**D**: anti-human PDGFRα. **E**–**H**: anti-human CD34. **I**–**L**: anti-human nestin. Pterygium and conjunctiva shared the same telocyte distribution pattern; however, in pterygium marked stromal TC hyperplasia was observed (**A**,**E**,**J**). In pterygium, strong immunoreactivity to PDGFRα, CD34, and nestin was localized underneath the epithelium along the basement membrane (**A**,**E**,**F**,**I**,**K**). In the stroma, immunoreactive TCs were widespread and arranged in perivascular sheaths around the newly formed vessels (**A**,**B**,**E**–**G**,**J**), as well as scattered in the stroma, where the TCs ran in bundles, parallel to the epithelium and simulating the course of elastic fibers (**A**,**E**,**J**). **C**: In the fibrotic areas, TCs were almost absent, but on the border of the cicatricial area, stellate PDGFRα immunoreactive TCs, with at least five extremely long, branched, dendritic-like processes, were detectable (arrows). **E**: The organization in parallel bundles went missing and was replaced with a wide TC network (arrows). **K**: High magnification of a nestin-positive TC, with very long telopodes, running along the basement membrane, was detectable. In conjunctiva, mild immunoreactivity to PDGFRα (**D**) and CD34 (**H**) was observed. No immunostaining to nestin (**L**) was detected in any cases. Scale bar: **A**–**J**,**L** = 50 µm; **K** = 20 µm.

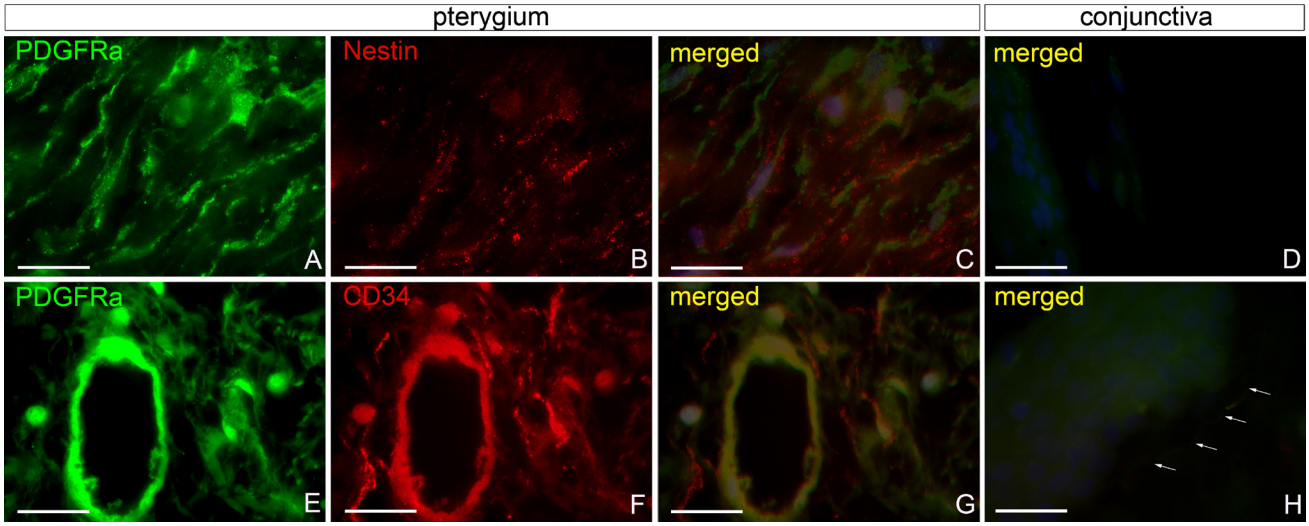

Figure 2. Double immunofluorescence labeling of TCs in pterygium and conjunctiva. **A-D**: double immunofluorescent reaction for PDGFRα (green) and nestin (red); **E-H**: double fluorescence immunolabeling for PDGFRα (green) and CD34 (red). Extensive colocalization (yellow) of PDGFRα and nestin (**C**) and PDGFRα and CD34 (**G**) in pterygium stromal telocytes was observed. Nestin was always expressed in a punctate/granular pattern (**B**,**C**). The scattered conjunctival stromal TCs always showed a PDGFRα+/nestin- (**D**) and PDGFRα+/CD34+ (**H**, arrows) immunophenotype. Nuclei (blue) are counterstained with 4′,6-diamidino-2-phenylindole (DAPI). Scale bar: **A**–**H** = 125 µm.

The conjunctival TCs (Table 3) showed mild immunoreactivity to PDGFRα (Figure 1D), CD34 (Figure 1H), and vimentin and weak staining to S100 and laminin; no immunostaining to nestin (Figure 1L), VEGF, and CD133 was detected in any case. Moreover, in pterygium (Figure 3A) and conjunctiva (Figure 3B), the TCs were always negative for c-kit. The only scattered c-kit-immunoreactive cells were morphologically identifiable as mast cells. Furthermore, only adventitial TCs of the perivascular sheaths showed marked staining to α-SMA (Figure 3G,H).

Transmission electron microscopy: In the electron transmission microscopy images of pterygium, TCs exhibited a small cell body of variable shapes (round, ovoid, spindle, or triangular) and frequently two to three remarkable Tps extending from the cell body. The Tps varied in length and width and were characterized by alternating thin (podomers)

Table 3. Semiquantitative analysis of immunostaining.

Antigens	Pterygium				Conjuntiva			
	SE-TCs	S-TCs	PVS-TCs	VE	SE-TCs	S-TCs	PVS-TCs	VE
PDGFRa	+++	+++	+++	+++	+	+	+	+
CD34	+++	+++	+++	+++	+	+	+	+
c-kit	-	-	-	-	-	-	-	-
Nestin	+++	+++	+++	+++	-	-	-	-
Vimentin	++	++	++	++	+	+	+	+
α-SMA	-	-	+++	-	-	-	++	-
Laminin	±	±	±	-	±	±	±	-
S100	±	±	±	-	±	±	±	-
VEGF	++	++	+++	+++	-	-	-	-
CD133	-	-	-	+++	-	-	-	-
CD31	-	-	-	+++	-	-	-	+++

SE-TCs, sub-epithelial telocytes. S-TCs, stromal telocytes. PVS-TCs, perivascular sheaths telocytes. VE, vascular endothelium. +++, strong immunoreactivity. ++, moderate immunoreactivity. +, mild immunoreactivity. ±, weak immunoreactivity. -, absence of immunoreactivity

and varicose (podoms) segments, giving the Tps a moniliform aspect; they appeared convoluted and sometimes branched. The nucleus, large, often irregular, and indented, occupied most part of the cell body. In the scant cytoplasm surrounding the nucleus, mitochondria, endoplasmic reticulum, Golgi apparatus, vesicles, different in size and shape, and small granules were well represented. Moreover, the typical cellular organelles, especially mitochondria and vesicles, were easily appreciable in the cytoplasm of Tps.

In pterygium, TCs were observed around blood vessels, scattered in the lamina propria (Figure 4A,B), and adjacent to the basement membrane of the epithelium (Figure 4C); focal heterocellular contact points between Tps and different types of cells were observed. In the stroma of pterygium, a small cell of about 5 µm, with a high nucleocytoplasmic ratio, indented heterochromatic nucleus, and low density of organelles, morphologically resembling a stem cell, next to a small blood vessel and in close relation with a Tp of a TC, was detected (Figure 4A). The cell showed at least eight heterocellular contact points with podoms, containing vesicles, of the Tp. Moreover, in all samples, several Tps forming sheaths around vessels were observed (Figure 4A,B). In the basal layer of pterygium epithelium, an epithelial stem cell, adjacent to Tps running parallel to the line of stromal–epithelial junction, was observed (Figure 4C). In mere observation, the morphological features and distribution of TCs in the pterygium samples (Figure 4) appeared similar to those observed in the conjunctiva samples (Figure 5).

DISCUSSION

TCs are an eclectic cell population hard to identify with conventional microscopy but very easy to reveal due to their characteristic ultrastructure. However, taking into account the constitutive limitations of two-dimensional (2D) electron microscopy, which cannot explore the whole surface of the cell body of the examined stromal cells and to ensure “a safe diagnosis of TCs” [34], in accordance with the recent publications by Neuhaus et al. [35] and Vannucchi et al. [36], the

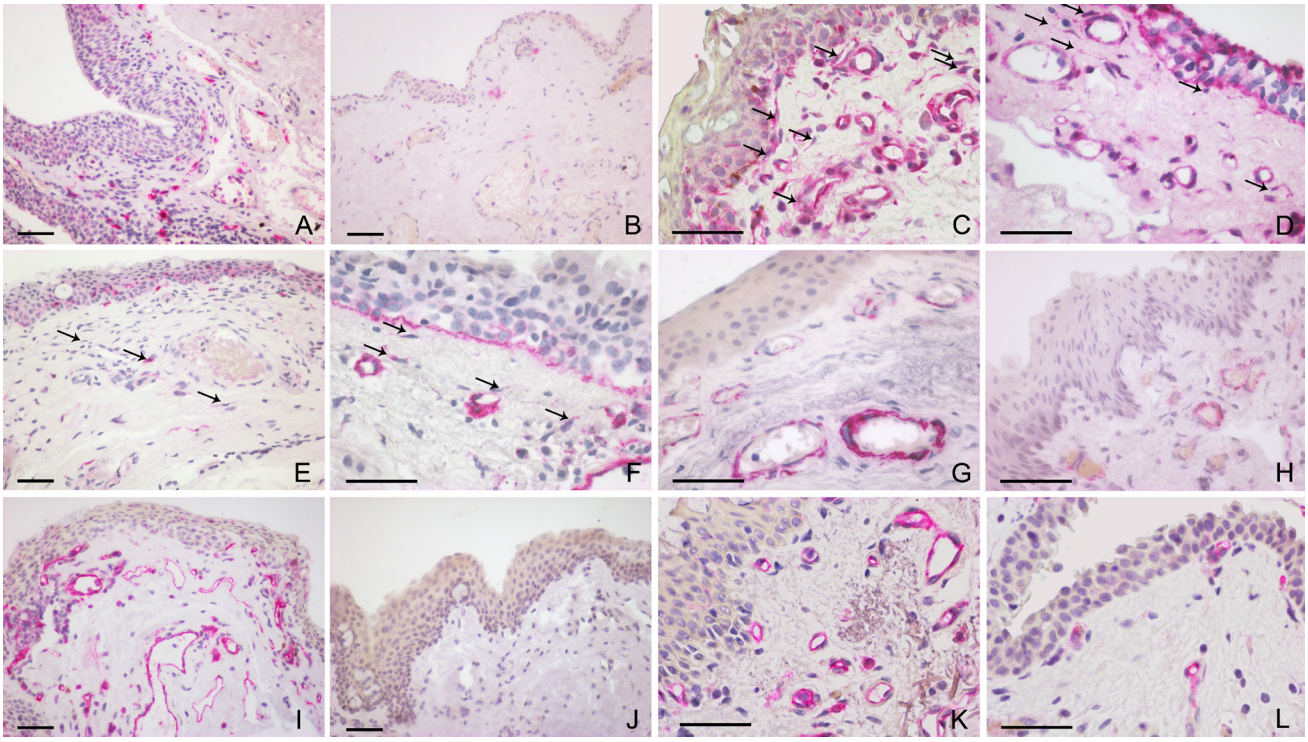

Figure 3. Immunohistochemical analysis of TCs in pterygium and conjunctiva. **A**,**B**: C-kit. **C**: Vimentin. **D**: VEGF. **E**: S100. F: Laminin. **G**,**H**: α-SMA. **I**,**J**: CD133. **K**,**L**: CD31. **A**,**C**–**G**,**I**,**K**: pterygium. **B**,**H**,**J**,**L**: conjunctiva. In pterygium (**A**) and conjunctiva (**B**), telocytes were always negative for c-kit; scattered c-kit-immunoreactive cells, morphologically identifiable as mast cells, were observable in the lamina propria. In pterygium, stromal TCs showed moderate immunostaining to vimentin (**C**, arrows) and VEGF (**D**, arrows); weak staining to S100 (**E**, arrows) and laminin (**F**, arrows) in a few stromal TCs was observed. **G**,**H**: Only adventitial TCs of the perivascular sheaths showed evident staining to α-SMA. **I**: CD133 immunoreactivity in pterygium TCs was completely absent and limited to the endothelial cells of neoformed blood vessels. No immunostaining in conjunctiva was observed (**J**). In pterygium (**K**) and conjunctiva (**L**), only endothelial cells showed immunoreactivity to CD31. Scale bar: **A**–**L** = 50 µm.

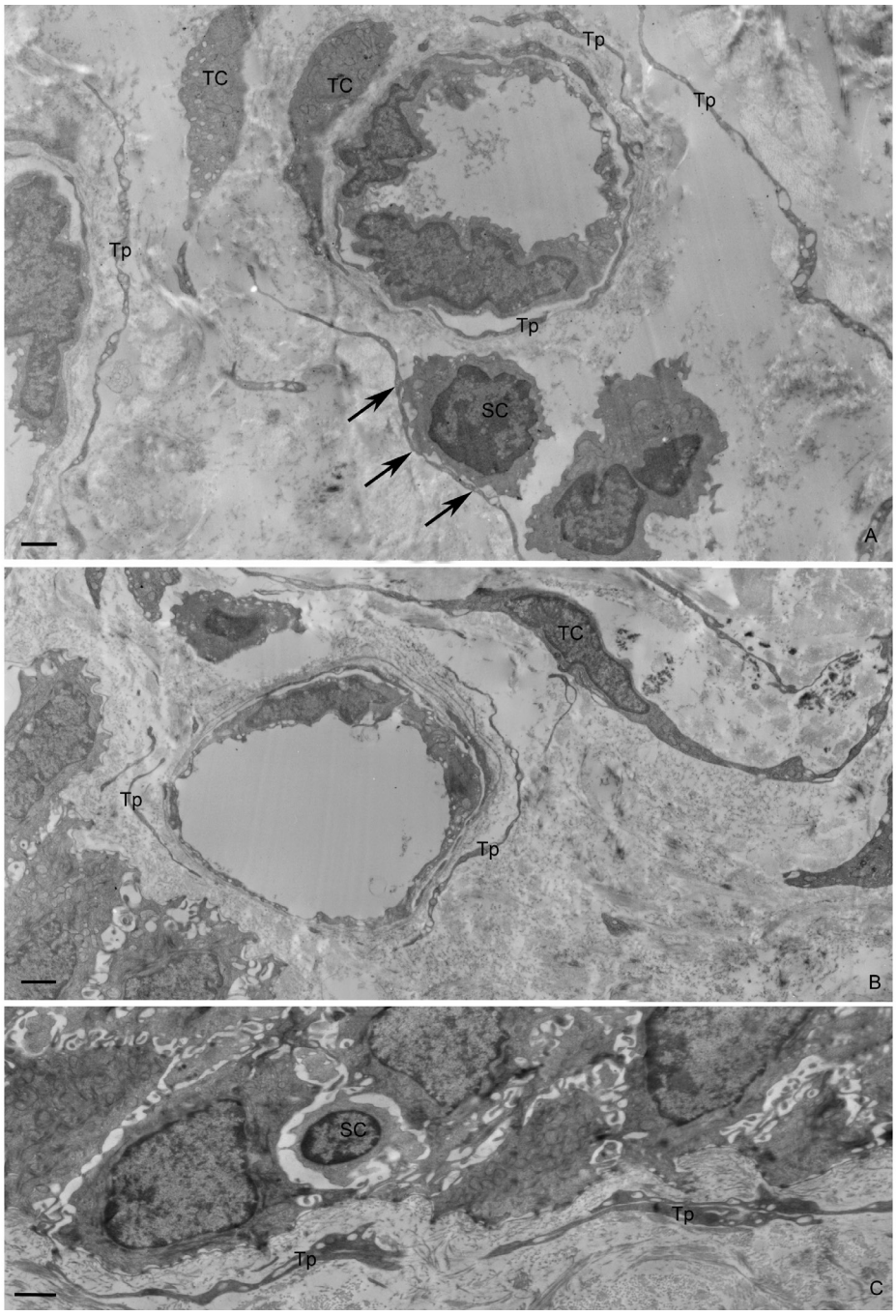

Figure 4. Transmission electron microscopy micrograph of pterygium. Elongated telocyte-like cells scattered in the stroma and around blood vessels were observed (**A**, **B**). Several long and thin Tps circling small blood vessels (**A**, **B**) and adjacent to the basement membrane (**C**) of the epithelium were detected. In **A**, a Tp that formed heterocellular contact points (arrows) with a morphologically resembling stem cell was observed. **C**: A basal epithelial stem cell adjacent to Tps running parallel to the line of the stromal–epithelial junction. Scale bar: **A**–**C** = 1 µm.

cells hereafter named "telocytes (TCs)" should, therefore, be seen as cells with "telocytic-like morphology" or "telocyte-like cells" [6].

TCs possess multiple phenotypes according to organ and animal species [2], because these cells can adapt in response to locally received signals and depending to their functions. TCs' most commonly expressed markers are PDGFRα, CD34, and c-kit. To better understand the role of TCs, ultrastructural identification must be coupled with immunohistochemistry. Although in the last few years TCs

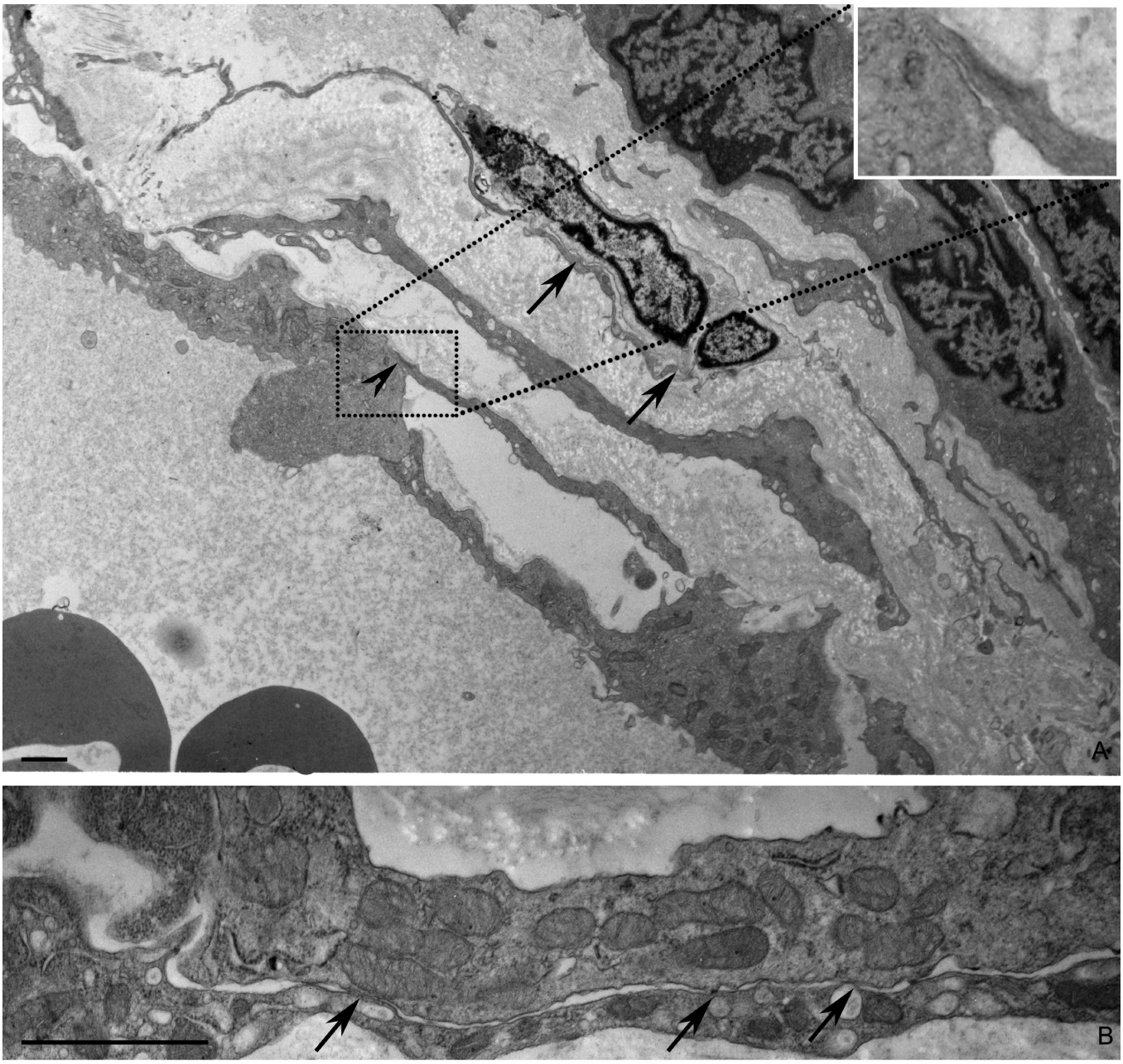

Figure 5. Transmission electron microscopy micrograph of conjunctiva. **A**: A stromal telocyte between two vessels and Tps of the perivascular sheaths were observed. Homocellular contact points (**A**, **B**, arrows) and a TC/endothelial cell heterocellular junction (**A**, arrowhead and high magnification inset) were observed. Scale bar: **A**–**B** = 1 µm.

have been widely studied in most tissues and organs, little is known about TCs in human conjunctiva, because the only available data are deduced from studies on the limbus and sclera [5,6], and, as far as we know, this is the first study to analyze and characterize TCs in pterygium. Thus, the aim of this study was twofold: to identify TCs in pterygium and to examine possible differences in TCs in terms of immunophenotype and/or localization between pterygium and normal conjunctiva, to evaluate possible involvement of TCs in pathogenesis of pterygium. We examined with immunohistochemistry a panel of 11 commercially available antibodies; among them, we demonstrated that in all pterygium samples TCs always express stemness markers, such as nestin, PDGFRα, and CD34, while c-kit was almost negative.

Nestin is a class VI intermediate filament protein first described in neuroepithelial stem cells and in nervous tissue

during embryogenesis [37], and in endothelial cells during angiogenesis [38], but not in differentiated adult cells. Moreover, nestin has been also detected in some tumors, such as gliomas [39] and glioblastomas [40], neuroblastomas [41], and angiosarcomas [42], and its positivity in vessels and tumoral cells may be considered a prognostic marker in melanoma and breast cancer [43,44]. To the best of our knowledge, only a few papers [45,46] have examined the distribution of nestin-positive cells in pterygium and conjunctiva. However, these studies focused on epithelium and stromal vessels; none described nestin distribution in the connective stroma. In the present study, the presence of TCs, always double positive for PDGFRα and nestin, was observable underneath the epithelium along the basement membrane and in the lamina propria. In the stroma, TCs were widespread and arranged in perivascular sheaths around the newly formed vessels, near the nerves, and scattered in the stroma, where the cells ran in bundles, parallel to the epithelium, similarly to that described by Marini and colleagues [47] in the corneal stroma, and possibly resembling the elastic fiber orientation. No expression of nestin was observed in conjunctival TCs, which always expressed a PDGFRα+/nestin- immunophenotype. As the expression of nestin has been documented in mesenchymal stem cells [48], perhaps the presence of nestin in pterygium TCs could be explained by reactivation of nestin in multipotential cells with regenerative potential [49], which might occur in pterygium under fibrotic conditions, to regenerate UVR-damaged stroma. This behavior is similar to that described for the regenerative potential of terminal Schwann cells (teloglia) of the neuromuscular junction after muscle denervation [50]. However, we should not be surprised as terminal Schwann cells and mesenchymal cells share a common embryonic origin from the neural crest [51].

In addition to nestin and PDGFRα, immunophenotype analysis revealed that CD34, another stemness marker, was always expressed in pterygium TCs; the expression of CD34 in conjunctiva, as PDGFRα, was weaker than in pterygium. PDGFRα+/Nestin+ and PDGFRα+/CD34+ phenotypes would not exclude that, in some cases, these markers may be referred to an endothelial lineage, as it has been shown in several papers on TCs [6,52-55]. In our opinion, the maintenance of a stemness immunophenotype in adulthood reinforces a previous hypothesis, which considered TCs adult stromal mesenchymal cells able "to differentiate in different cell lines, when necessary" [56,57] and supports our idea about the involvement of TCs in pterygium stromal repair, acting as nurse cells through stem cell modulation. To further support this hypothesis, in the stroma of a pterygium sample, treated for the ultrastructural analysis, we observed a small cell of about 5 µm, with a high nucleocytoplasmic ratio, indented heterochromatic nucleus, and low density of organelles, morphologically resembling a stem cell, next to a small blood vessel and in close relation with a Tp of a TC. This small cell, very similar to those described by Luesma et al. [5] in the stromal stem cell niches located in the corneoscleral junction, showed at least eight points of heterocellular contact with podoms, containing vesicles, of the Tp, in agreement with a previous study by Gherghiceanu and Popescu [58]. These junctions are probably necessary for stem cells to migrate between different layers of the eye, sliding along the dynamic scaffold created by the Tps of the TCs, recalling migrating neurons along the processes of radial glial cells during the development of the brain [59]. However, this mechanism in conjunctiva/pterygium must be elucidated, and further studies are required to clarify the characteristics of these junctions. Furthermore, in the basal layer of the pterygium epithelium, we observed an epithelial stem cell adjacent to Tps running along the basal membrane, probably because of the role of TCs in homeostatic renewal of the conjunctival epithelium [60].

More than ten years ago, other researchers [26-28] demonstrated the presence of progenitor cells in pterygium stroma, but these cells had not been classified, as the term "telocyte" was proposed in 2010 by Popescu and Faussone-Pellegrini [1]. In the present study, in addition to immunoreactivity to nestin, PDGFRα, and CD34, pterygium TCs were negative for c-kit, probably because of its inconsistent expression in TCs. The only scattered c-kit-immunoreactive cells were morphologically identifiable as mast cells, as described by Vannucchi et al. [57,61] in the human gastrointestinal tract and urinary bladder. CD133 immunoreactivity in TCs was totally absent and limited to the endothelial cells of neoformed blood vessels, which showed staining also for the pan-endothelial marker CD31, PDGFRα, CD34, nestin, vimentin, and VEGF. As expected, the TCs did not display any staining for CD31, in agreement with several authors [53,62,63], who stated that a $CD34^{+}/CD31^{-}$ immunophenotype would prevent doubtful interpretation between TCs and endothelial cells. Although we cannot completely exclude with 2D transmission electron microscopy that the observed cells are endothelial cells, we can claim their TC-like nature by the immunophenotypic characterization, at least in the context of conjunctiva/pterygium stroma.

Furthermore, in pterygium TCs showed moderate immunoreactivity to vimentin and VEGF, in agreement with previous data [64,65], while weak staining for S100 and laminin in scattered stromal telocyte-like cells was detected. It is well-established that a key role in the development of pterygium is represented by the intense angiogenic activity,

triggered by chronic UVR-B exposure, responsible for the upregulation of VEGF induced by oxidative stress, hypoxia, and inflammation [66]. In pterygium, our tagging of stromal VEGF-positive cells as TCs might confirm their involvement as causative agents in the neoangiogenic activity, perhaps through a paracrine secretion.

S100 protein was described in pancreas interstitial cells of Cajal (later identified as TCs) [67], and in the epicardium [68], and the contribution of S100 in the secretory activities of TCs was postulated in the uterine tube [69]. In the present study, S100-positive TCs were scattered in the lamina propria of pterygium and showed weak, much lower than that of the internal controls represented by stromal nerves, epithelial melanocytes, and Langerhans' cells. However, this result is not surprising, because it overlaps with that described in our first paper about pterygium [14]. Moreover, in pterygium only the adventitial TCs of the perivascular sheaths showed marked staining to α-SMA, probably because of the presence of two populations of TCs [61] with different contractile properties. This result was confirmed in conjunctiva.

Regarding TC distribution, in the study we observed that normal conjunctiva and pterygium shared the same pattern of localization; however, we observed marked TC hyperplasia in the pterygium stroma, probably due to hypoxia and to the inflammatory process, which are responsible for the migration of mesenchymal stem cells from their niches through the circulatory system [70]. In addition, in certain areas the arrangement in parallel bundles went missing and was replaced with a wide TC network, as reported by Diaz-Flores et al. [71]. Moreover, in agreement with the research by Fu and colleagues [72] in human liver fibrosis, in those areas of pterygium in which the degeneration of the elastic fibers reached the highest level, the stroma became fibrotic and turned into cicatricial tissue, where TCs and fibroblasts were almost absent. Furthermore, on the border of the cicatricial area, we observed the presence of stellate TCs with at least five extremely long, branched, and interconnected "dendritic-like processes", already called "modified Tps" [71]; this finding is in agreement with previous observations by Erdag et al. [73] in other benign tumors, probably as a result of morphological alterations occurring in TCs during inflammatory processes [74]. However, this observation in pterygium must be elucidated further.

In conclusion, 2D transmission electron microscopy seems to be insufficient to distinguish TCs from other CD34+ stromal cells. Thus, it seems reasonable to call TCs "telocyte-like cells", based on their morphological characteristics, together with their immunoreactivity to CD34, PDGFRα [75], and nestin [52]. Therefore, TC-like cells in pterygium may represent a multipotential subpopulation of relatively immature cells with regenerative potential, and the expression of nestin may suggest the possible involvement of TC-like cells as active players in the regeneration of UVR-damaged stroma and vascular remodeling. The fibrosis and the absence of TC-like cells in the cicatricial area might represent the failure of the process of regeneration, due to cell modification induced by inflammation.

ACKNOWLEDGMENTS

The authors are thankful to Mrs. Maria Itala Mosso for her skillful technical assistance. The study was supported by grants from the Fondo Integrativo per la Ricerca (FIR) of the University of Cagliari, Italy. None of the authors have financial or other types of competing interests. Some of the results of this work were presented at the 71st National Congress of the Italian Society of Anatomy and Histology (SIAI) in Taormina, Italy [abstract published in: It J Anat Embryol. 2017; 122(1):142].

REFERENCES

1. Popescu LM, Faussone-Pellegrini MS. TELOCYTES - a case of serendipity: the winding way from Interstitial cells of Cajal (ICC), via Interstitial Cajal-Like Cells (ICLC) to TELOCYTES. J Cell Mol Med 2010; 14:729-40. [PMID: 20367664].

2. Cretoiu D, Radu BM, Banciu A, Banciu DD, Cretoiu SM. Telocytes heterogeneity: From cellular morphology to functional evidence. Semin Cell Dev Biol 2017; 64:26-39. [PMID: 27569187].

3. Ibba-Manneschi L, Rosa I, Manetti M. Telocyte implications in human pathology: An overview. Semin Cell Dev Biol 2016; 55:62-9. [PMID: 26805444].

4. Popescu LM, Gherghiceanu M, Cretoiu D, Radu E. The connective connection: interstitial cells of Cajal (ICC) and ICC-like cells establish synapses with immunoreactive cells. Electron microscope study in situ. J Cell Mol Med 2005; 9:714-30. [PMID: 16202219].

5. Luesma MJ, Gherghiceanu M, Popescu LM. Telocytes and stem cells in limbus and uvea of mouse eye. J Cell Mol Med 2013; 17:1016-24. [PMID: 23991685].

6. Petrea CE, Rusu MC, Mănoiu VS, Vrapciu AD. Telocyte-like cells containing Weibel-Palade bodies in rat lamina fusca. Ann Anat 2018; 218:88-94. [PMID: 29655846].

7. Demurtas P, Orrù G, Coni P, Minerba L, Corrias M, Sirigu P, Zucca I, Demurtas E, Maxia C, Piras F, Murtas D, Lai S, Perra MT. Association between the ACE insertion/deletion polymorphism and pterygium in Sardinian patients: a population-based case-control study. BMJ Open 2014; 4:e005627-[PMID: 25341451].

8. Lin A, Stern G. Correlation between pterygium size and induced corneal astigmatism. Cornea 1998; 17:28-30. [PMID: 9436877].

9. Dushku N, Reid TW. P53 expression in altered limbal basal cells of pingueculae, pterygia, and limbal tumors. Curr Eye Res 1997; 16:1179-92. [PMID: 9426949].

10. Tan DT, Lim AS, Goh HS, Smith DR. Abnormal expression of the p53 tumor suppressor gene in the conjunctiva of patients with pterygium. Am J Ophthalmol 1997; 123:404-5. [PMID: 9063255].

11. Perra MT, Colombari R, Maxia C, Zucca I, Piras F, Corbu A, Bravo S, Scarpa A, Sirigu P. Finding of conjunctival melanocytic pigmented lesions within pterygium. Histopathology 2006; 48:387-93. [PMID: 16487360].

12. Chui J, Coroneo MT, Tat LT, Crouch R, Wakefield D, Di Girolamo N. Ophthalmic pterygium: a stem cell disorder with premalignant features. Am J Pathol 2011; 178:817-27. [PMID: 21281814].

13. Di Girolamo N, McCluskey P, Lloyd A, Coroneo MT, Wakefield D. Expression of MMPs and TIMPs in human pterygia and cultured pterygium epithelial cells. Invest Ophthalmol Vis Sci 2000; 41:671-9. [PMID: 10711680].

14. Perra MT, Maxia C, Zucca I, Piras F, Sirigu P. Immunohistochemical study of human pterygium. Histol Histopathol 2002; 17:139-49. [PMID: 11813864].

15. Maxia C, Perra MT, Demurtas P, Minerba L, Murtas D, Piras F, Cabrera R, Ribatti D, Sirigu P. Relationship between the expression of cyclooxygenase-2 and survivin in primary pterygium. Mol Vis 2009; 15:458-63. [PMID: 19247455].

16. Demurtas P, Di Girolamo N, Corrias M, Zucca I, Maxia C, Diana A, Piras F, Lai S, Sirigu P, Perra MT. Immunohistochemical analysis of angiotensin converting enzyme in Sardinian pterygium. Histol Histopathol 2013; 28:759-66. [PMID: 23208948].

17. Tan DT, Tang WY, Liu YP, Goh HS, Smith DR. Apoptosis and apoptosis related gene expression in normal conjunctiva and pterygium. Br J Ophthalmol 2000; 84:212-6. [PMID: 10655200].

18. Di Girolamo N, Kumar RK, Coroneo MT, Wakefield D. UVB-mediated induction of interleukin-6 and −8 in pterygia and cultured human pterygium epithelial cells. Invest Ophthalmol Vis Sci 2002; 43:3430-7. [PMID: 12407153].

19. Kria L, Ohira A, Amemiya T. Growth factors in cultured pterygium fibroblasts: immunohistochemical and ELISA analysis. Graefes Arch Clin Exp Ophthalmol 1998; 236:702-8. [PMID: 9782432].

20. Ribatti D, Nico B, Perra MT, Maxia C, Piras F, Murtas D, Crivellato E, Sirigu P. Correlation between NGF/TrkA and microvascular density in human pterygium. Int J Exp Pathol 2009; 90:615-20. [PMID: 19758420].

21. Detorakis ET, Drakonaki EE, Spandidos DA. Molecular genetic alterations and viral presence in ophthalmic pterygium. Int J Mol Med 2000; 6:35-41. [PMID: 10851263].

22. Tsai YY, Cheng YW, Lee H, Tsai FJ, Tseng SH, Lin CL, Chang KC. Oxidative DNA damage in pterygium. Mol Vis 2005; 11:71-5. [PMID: 15692461].

23. Kim KW, Ha HS, Kim JC. Ischemic tissue injury and progenitor cell tropism: significant contributors to the pathogenesis of pterygium. Histol Histopathol 2015; 30:311-20. [PMID: 25314135].

24. Riau AK, Wong TT, Beuerman RW, Tong L. Calcium-binding S100 protein expression in pterygium. Mol Vis 2009; 15:335-42. [PMID: 19223989].

25. Maxia C, Murtas D, Corrias M, Zucca I, Minerba L, Piras F, Marinelli C, Perra MT. Vitamin D and vitamin D receptor in patients with ophthalmic pterygium. Eur J Histochem 2017; 61:2837-[PMID: 29313597].

26. Ye J, Song YS, Kang SH, Yao K, Kim JC. Involvement of bone marrow-derived stem and progenitor cells in the pathogenesis of pterygium. Eye (Lond) 2004; 18:839-43. [PMID: 15002023].

27. Lee JK, Kim JC. Progenitor cells in healing after pterygium excision. Yonsei Med J 2007; 48:48-54. [PMID: 17326245].

28. Lee JK, Song YS, Ha HS, Park JH, Kim MK, Park AJ, Kim JC. Endothelial progenitor cells in pterygium pathogenesis. Eye (Lond) 2007; 21:1186-93. [PMID: 16732212].

29. Bandrowski A, Brush M, Grethe JS, Haendel MA, Kennedy DN, Hill S, Hof PR, Martone ME, Pols M, Tan SC, Washington N, Zudilova-Seinstra E, Vasilevsky N. RINL Resource Identification Initiative. The Resource Identification Initiative: a cultural shift in publishing. Brain Behav 2015; 6:e00417-[PMID: 27110440].

30. Marini M, Manetti M, Rosa I, Ibba-Manneschi L, Sgambati E. Telocytes in human fetal skeletal muscle interstitium during early myogenesis. Acta Histochem 2018; 120:397-404. [PMID: 29724455].

31. Lai S, Piras F, Spiga S, Perra MT, Minerba L, Piga M, Mura E, Murtas D, Demurtas P, Corrias M, Maxia C, Ferreli C, Sirigu P. Nestin and vimentin colocalization affects the subcellular location of glucocorticoid receptor in cutaneous melanoma. Histopathology 2013; 62:487-98. [PMID: 23072594].

32. Murtas D, Piras F, Minerba L, Maxia C, Ferreli C, Demurtas P, Lai S, Mura E, Corrias M, Sirigu P, Perra MT. Activated Notch1 expression is associated with angiogenesis in cutaneous melanoma. Clin Exp Med 2015; 15:351-60. [PMID: 25034654].

33. Lilliu MA, Loy F, Cossu M, Solinas P, Isola R, Isola M. Morphometric study of diabetes related alterations in human parotid gland and comparison with submandibular gland. Anat Rec (Hoboken) 2015; 298:1911-8. [PMID: 26264892].

34. Rusu MC, Nicolescu MI, Jianu AM, Lighezan R, Mănoiu VS, Păduraru D. Esophageal telocytes and hybrid morphologies. Cell Biol Int 2012; 36:1079-88. [PMID: 22931066].

35. Neuhaus J, Schröppel B, Dass M, Zimmermann H, Wolburg H, Fallier-Becker P, Gevaert T, Burkhardt CJ, Do HM, Stolzenburg JU. 3D-electron microscopic characterization of

interstitial cells in the human bladder upper lamina propria. Neurourol Urodyn 2018; 37:89-98. [PMID: 28370277].

36. Vannucchi MG, Traini C. The telocytes/myofibroblasts 3-D network forms a stretch receptor in the human bladder mucosa. Is this structure involved in the detrusor overactive diseases? Ann Anat 2018; 218:118-23. [PMID: 29654819].

37. Lendahl U, Zimmerman LB, McKay RD. CNS stem cells express a new class of intermediate filament protein. Cell 1990; 60:585-95. [PMID: 1689217].

38. Mokrý J, Cízková D, Filip S, Ehrmann J, Osterreicher J, Kolár Z, English D. Nestin expression by newly formed human blood vessels. Stem Cells Dev 2004; 13:658-64. [PMID: 15684833].

39. Sugawara K, Kurihara H, Negishi M, Saito N, Nakazato Y, Sasaki T, Takeuchi T. Nestin as a marker for proliferative endothelium in gliomas. Lab Invest 2002; 82:345-51. [PMID: 11896213].

40. Veselska R, Kuglik P, Cejpek P, Svachova H, Neradil J, Loja T, Relichova J. Nestin expression in the cell lines derived from glioblastoma multiforme. BMC Cancer 2006; 6:32-[PMID: 16457706].

41. Thomas SK, Messam CA, Spengler BA, Biedler JL, Ross RA. Nestin is a potential mediator of malignancy in human neuroblastoma cells. J Biol Chem 2004; 279:27994-9. [PMID: 15117961].

42. Krupkova O Jr, Loja T, Redova M, Neradil J, Zitterbart K, Sterba J, Veselska R. Analysis of nuclear nestin localization in cell lines derived from neurogenic tumors. Tumour Biol 2011; 32:631-9. [PMID: 21340483].

43. Piras F, Perra MT, Murtas D, Minerba L, Floris C, Maxia C, Demurtas P, Ugalde J, Ribatti D, Sirigu P. The stem cell marker nestin predicts poor prognosis in human melanoma. Oncol Rep 2010; 23:17-24. [PMID: 19956860].

44. Piras F, Ionta MT, Lai S, Perra MT, Atzori F, Minerba L, Pusceddu V, Maxia C, Murtas D, Demurtas P, Massidda B, Sirigu P. Nestin expression associates with poor prognosis and triple negative phenotype in locally advanced (T4) breast cancer. Eur J Histochem 2011; 55:215-20. [PMID: 22297445].

45. Wen D, Wang H, Heng BC, Liu H. Increased expression of nestin in human pterygial epithelium. Int J Ophthalmol 2013; 6:259-63. [PMID: 23826515].

46. Tonthat CV, Di Girolamo N. Nestin expression in pterygia: potential role in angiogenesis. Br J Ophthalmol 2014; 98:801-7. [PMID: 24008823].

47. Marini M, Mencucci R, Rosa I, Favuzza E, Guasti D, Ibba-Manneschi L, Manetti M. Telocytes in normal and keratoconic human cornea: an immunohistochemical and transmission electron microscopy study. J Cell Mol Med 2017; 21:3602-11. [PMID: 28714595].

48. Wislet-Gendebien S, Hans G, Leprince P, Rigo JM, Moonen G, Rogister B. Plasticity of cultured mesenchymal stem cells: switch from nestin-positive to excitable neuron-like phenotype. Stem Cells 2005; 23:392-402. [PMID: 15749934].

49. Wiese C, Rolletschek A, Kania G, Blyszczuk P, Tarasov KV, Tarasova Y, Wersto RP, Boheler KR, Wobus AM. Nestin expression–a property of multi-lineage progenitor cells? Cell Mol Life Sci 2004; 61:2510-22. [PMID: 15526158].

50. Kang H, Tian L, Son YJ, Zuo Y, Procaccino D, Love F, Hayworth C, Trachtenberg J, Mikesh M, Sutton L, Ponomareva O, Mignone J, Enikolopov G, Rimer M, Thompson W. Regulation of the intermediate filament protein nestin at rodent neuromuscular junctions by innervation and activity. J Neurosci 2007; 27:5948-57. [PMID: 17537965].

51. Thomas W. Sadler. Chapter 6. Third to Eighth Weeks: The Embryonic Period. In: Langman's Medical Embryology, 13th edition. Wolters Kluver; 2015. p. 71–94.

52. Grigoriu F, Hostiuc S, Vrapciu AD, Rusu MC. Subsets of telocytes: the progenitor cells in the human endocardial niche. Rom J Morphol Embryol 2016; 57:767-74. [PMID: 27833970].

53. Petrea CE, Crăiţoiu Ş, Vrapciu AD, Mănoiu VS, Rusu MC. The telopode- and filopode-projecting heterogeneous stromal cells of the human sclera niche. Ann Anat 2018; 218:129-40. [PMID: 29694850].

54. Rusu MC, Hostiuc S, Vrapciu AD, Mogoantă L, Mănoiu VS, Grigoriu F. Subsets of telocytes: Myocardial telocytes. Ann Anat 2017; 209:37-44. [PMID: 27777113].

55. Rusu MC, Mănoiu VS, Creţoiu D, Creţoiu SM, Vrapciu AD. Stromal cells/telocytes and endothelial progenitors in the perivascular niches of the trigeminal ganglion. Ann Anat 2018; 218:141-55. [PMID: 29680777].

56. Pieri L, Vannucchi MG, Faussone-Pellegrini MS. Histochemical and ultrastructural characteristics of an interstitial cell type different from ICC and resident in the muscle coat of human gut. J Cell Mol Med 2008; 12:1944-55. [PMID: 19145703].

57. Vannucchi MG, Traini C, Manetti M, Ibba-Manneschi L, Faussone-Pellegrini MS. Telocytes express PDGFRα in the human gastrointestinal tract. J Cell Mol Med 2013; 17:1099-108. [PMID: 24151977].

58. Gherghiceanu M, Popescu LM. Cardiac telocytes - their junctions and functional implications. Cell Tissue Res 2012; 348:265-79. [PMID: 22350946].

59. Rakic P. Cell migration and neuronal ectopias in the brain. In: Bergsma D, editor. Morphogenesis and Malformation of the Face and Brain (Birth Defects: Original Series). New York: Alan Liss; 1975. p 95–129.

60. Shoshkes-Carmel M, Wang YJ, Wangensteen KJ, Tóth B, Kondo A, Massassa EE, Itzkovitz S, Kaestner KH. Subepithelial telocytes are an important source of Wnts that supports intestinal crypts. Nature 2018; 557:242-6. [PMID: 29720649].

61. Vannucchi MG, Traini C, Guasti D, Del Popolo G, Faussone-Pellegrini MS. Telocytes subtypes in human urinary bladder. J Cell Mol Med 2014; 18:2000-8. [PMID: 25139461].

62. Manetti M, Rosa I, Messerini L, Guiducci S, Matucci-Cerinic M, Ibba-Manneschi L. A loss of telocytes accompanies

fibrosis of multiple organs in systemic sclerosis. J Cell Mol Med 2014; 18:253-62. [PMID: 24467430].

63. Díaz-Flores L, Gutiérrez R, Sáez FJ, Díaz-Flores L Jr, Madrid JF. Telocytes in neuromuscular spindles. J Cell Mol Med 2013; 17:457-65. [PMID: 23621814].

64. Nubile M, Curcio C, Lanzini M, Calienno R, Iezzi M, Mastropasqua A, Di Nicola M, Mastropasqua L. Expression of CREB in primary pterygium and correlation with cyclin D1, ki-67, MMP7, p53, p63 Survivin and Vimentin. Ophthalmic Res. 2013; 50:99-107. [PMID: 23838680].

65. Bianchi E, Scarinci F, Grande C, Plateroti R, Plateroti P, Plateroti AM, Fumagalli L, Capozzi P, Feher J, Artico M. Immunohistochemical profile of VEGF, TGF-β and PGE_2 in human pterygium and normal conjunctiva: experimental study and review of the literature. Int J Immunopathol Pharmacol 2012; 25:607-15. [PMID: 23058011].

66. Lee DH, Cho HJ, Kim JT, Choi JS, Joo CK. Expression of vascular endothelial growth factor and inducible nitric oxide synthase in pterygia. Cornea 2001; 20:738-42. [PMID: 11588427].

67. Popescu LM, Hinescu ME, Ionescu N, Ciontea SM, Cretoiu D, Ardelean C. Interstitial cells of Cajal in pancreas. J Cell Mol Med 2005; 9:169-90. [PMID: 15784175].

68. Popescu LM, Manole CG, Gherghiceanu M, Ardelean A, Nicolescu MI, Hinescu ME, Kostin S. Telocytes in human epicardium. J Cell Mol Med 2010; 14:2085-93. [PMID: 20629996].

69. Abd-Elhafeez HH, Soliman SA. New description of telocyte sheaths in the bovine uterine tube: an immunohistochemical and scanning microscopic study. Cells Tissues Organs 2017; 203:295-315. [PMID: 28030857].

70. Rochefort GY, Delorme B, Lopez A, Herault O, Bonnet P, Charbord P, Eder V, Domenech J. Multipotential mesenchymal stem cells are mobilized into peripheral blood by hypoxia. Stem Cells 2006; 24:2202-8. [PMID: 16778152].

71. Díaz-Flores L, Gutiérrez R, Díaz-Flores L Jr, Goméz MG, Sáez FJ, Madrid JF. Behaviour of telocytes during physiopathological activation. Semin Cell Dev Biol 2016; 55:50-61. [PMID: 26826526].

72. Fu S, Wang F, Cao Y, Huang Q, Xiao J, Yang C, Popescu LM. Telocytes in human liver fibrosis J Cell Mol Med 2015; 19:676-83. [PMID: 25661250].

73. Erdag G, Qureshi HS, Patterson JW, Wick MR. CD34-positive dendritic cells disappear from scars but are increased in pericicatricial tissue. J Cutan Pathol 2008; 35:752-6. [PMID: 18331567].

74. Yang XJ, Yang J, Liu Z, Yang G, Shen ZJ. Telocytes damage in endometriosis-affected rat oviduct and potential impact on fertility. J Cell Mol Med 2015; 19:452-62. [PMID: 25388530].

75. Cretoiu SM. Telocytes in focus. Semin Cell Dev Biol 2016; 55:1-2. [PMID: 27288886].

Articles are provided courtesy of Emory University and the Zhongshan Ophthalmic Center, Sun Yat-sen University, P.R. China. The print version of this article was created on 29 December 2018. This reflects all typographical corrections and errata to the article through that date. Details of any changes may be found in the online version of the article.